Temperature Coefficients of Rates of Ethyl Radical Reactions with HBr and Br in the 228−368 K Temperature Range at Millitorr Pressures

Otto Dobis and Sidney W. Benson*

Loker Hydrocarbon Research Institute, University of Southern California, University Park, Los Angeles, California 90089-1661

Received: March 4, 1997; In Final Form: June 10, 1997[⊗]

The rates of the reactions of ethyl radicals with HBr (k_7) and with Br atoms (k_8) have been measured in the temperature range 228−368 K at millitorr pressures using the very low pressure reactor (VLPR) technique. The Arrhenius function for the H atom abstraction reaction is found to be $k_7 = (1.43 \pm 0.06) \times 10^{-12}$ exp[−(444 ± 26)/*RT*] cm^3/(molecule s), while the ethyl radical disproportionation with Br atom shows no temperature dependence. Its average value over the entire temperature range is $k_8 = (1.18 \pm 0.05) \times 10^{-11}$ cm^3/(molecule s). Reaction 7 is significantly slower than has been reported in the only other two direct measurements, both finding a negative activation energy for k_7 of from −1.0 to −1.1 kcal/mol. The small positive activation energy found in this work for k_7 fits standard models for H atom metathesis. Combination with all known kinetic information for ethane bromination gives an average reaction enthalpy of $\Delta H°_7 = 13.0 \pm 0.2$ kcal/mol using both the second- and third-law thermochemical calculations. It sets the heat of ethyl radical formation to $\Delta_f H°(C_2H_5) = 28.40 \pm 0.25$ kcal/mol and the bond dissociation enthalpy, $DH°(C_2H_5-H) = 100.5 \pm 0.3$ kcal/mol.

Introduction

Important complex chemical processes, like combustion, petroleum refining, and hydrocarbon cracking, as well as atmospheric chemistry, like smog formation, ozone layer stability, and chemical vapor deposition, are made up of a large number of elementary steps involving radical−radical and/or radical−molecule interactions which usually determine the overall rates or dynamics of these processes. The interpretation and modeling of these complex processes require a reliable data base of kinetic parameters for the elementary steps involved, that is, a large, accurate set of rate constants and also thermochemical parameters for the reactants, products, and intermediates. While such a data base is well established for molecular thermochemistry and has been reviewed recently,[1] the thermochemical data base for intermediates, even for simple organic radicals, is still somewhat elusive in spite of extensive experimental and theoretical effort for the past few decades. The lack of broad consensus is mainly related to the very real experimental difficulties in realizing equilibrium for reversible chemical reactions involving these short-lived intermediates.

Traditionally, the halogen (X) atom−hydrogen halide chemical equilibria

$$X + RH \overset{a}{\rightleftharpoons} HX + R$$

have been studied[2] most extensively and provided the first systematic set of data on the standard heat of formations of radicals, $\Delta_f H°(R)$, and bond dissociation enthalpies $DH°(R-H)$. From these early studies of the kinetics of bromination and iodination (X = Br or I), $\Delta_f H°(R)$ was calculated assuming that E_{-a} is very small[3] (0−3 kcal/mol) and within the scatter of the reported values of the activation energy of the forward reaction.

Some controversy arose when other chemical equilibrium studies at higher temperatures such as bond fission−radical recombination[4]

$$R-R' \overset{b}{\rightleftharpoons} R + R'$$

and the decomposition of alkyl radicals[5]

$$R \overset{c}{\rightleftharpoons} \text{olefin} + CH_3/H$$

yielded higher values for $\Delta_f H°(R)$ by 1−3 kcal/mol. Although the three different types of equilibria are much more complicated than the simplified schemes *a*, *b*, and *c* suggest[6] and appropriate experimental conditions were used to minimize the influence of side reactions and pressure dependence, it was proposed[4] to check the zero backward activation energy assumption for the halogenation equilibrium by direct measurements of reaction −*a*. Using a powerful UV laser flash of 193, 248, or 266 nm to decompose suitable radical precursors, the kinetics of the reverse reaction −*a* was studied in rapid, time-resolved flow tube experiments.[7−9] Investigations were carried out in a systematic way by generating CH_3, C_2H_5, *i*-C_3H_7, *s*-C_4H_9, and *t*-C_4H_9 radicals, and the rate constants and their temperature dependence for the radical consumption rates were measured in reactions with HBr[7,8] and with HI.[9] The results were surprising as all 10 reactions have shown very fast rates enhanced by negative activation energies of from −0.3 to −1.9 kcal/mol. Except in the case of *s*-C_4H_9, these activation energies are slightly more negative for R + HBr than for R + HI reactions. It was proposed that, unlike the forward reaction *a*, the reverse reaction is not an H metathesis, but a two-step chemical activation process.[10]

Without any proof for this two-step mechanism, it was incorporated into equilibria *a*, leading to an excessively high value of $\Delta H°_a$ when combined with known thermal bromination rate measurements[11−14] for the forward reaction *a*, which in terms of $\Delta_f H°(R)$ actually overshot the targets set by Tsang.[5] Therefore, the forward bromination reactions were reinvestigated using laser flash generation of Br atoms[7,15] and it was found that the forward reaction rates are also faster, mainly due to

[⊗] Abstract published in *Advance ACS Abstracts,* August 1, 1997.

S1089-5639(97)00822-0 CCC: $14.00

lower activation energies by about 1 kcal/mol. Equilibria *a* were then described by faster rates in both directions and new "direct" values for $\Delta_f H°(R)$ and $DH°(R-H)$ presented[16] as free from earlier zero or low positive activation energy assumptions for the reverse reaction $-a$. These new values have been compiled as critical data in recent editions of *CRC Handbook of Chemistry and Physics* (74−76th eds. of 1993−1996).

Apart from the thermochemical consequences derived from new K_a values of faster opposing reaction rates, the proposed two-step transition state mechanism for the backward reaction $-a$ is of special interest by itself. It makes a sharp break with our conventional understanding of an entire class of H abstraction reactions, and so far, this new concept has not been subjected to a thorough experimental or theoretical testing. A few recent studies, which found positive activation energies, either did not explore the controversy, like the competitive bromination of RCl species,[17] or arrived at a vague, conciliatory conclusion, like the combined *ab initio* calculation of CH_3 + HBr reaction[18] and the two-channel RRKM calculation of *t*-C_4H_9 + HI reaction.[19] The latter was misinterpreted as a support for the two-step mechanism[10] for that reaction.

Almost all earlier studies of the relative rate constants for

$$R + HX \xrightarrow{-a} RH + H$$

$$R + X_2 \xrightarrow{d} RX + X$$

have shown that $E_{-a} - E_d \geq 0$, but in recent investigations, it is found only for R = CH_3 in both cases when X = Cl[20,45] or Br.[7,21] In all other cases of radicals from C_2H_5 to C_4H_9 and of X = Br, $E_{-a} - E_d < 0$, ranging from −0.27 for R = C_2H_5 to −0.90 kcal/mol for the *tert*-butyl radical,[7,21,23] as E_d is less negative than E_{-a}. It is difficult to imagine why reaction *d* would have any restriction on proceeding by a direct metathesis path.

Another difficulty not addressed occurs in the case of the reaction of H atoms with RX (X = Br, I)[44] where the products are uniquely R + HX. The two-step mechanism[10] would predict the more stable RH + X product channel.

In our preceding paper,[22] we reported on the investigation of the C_2H_5 + HBr reaction rate at 298 K carried out in the very low pressure reactor (VLPR) system, using as a thermal ethyl radical source the C_2H_6 + Cl reaction. This experimental technique for the first time permits the measurement of all reaction rates both first and second orders. No side reaction can escape undetected over the detection limit of our sensitive mass spectrometric analytical method. Simultaneous measurements of *all* reactant and product concentrations give excellent mass balances for all species to 98 ± 2% accuracy.

Our rate constant value[22] for k_7 was found to be 14 times smaller than those reported over the past 6 years[7,23] which employed laser flash photolysis for radical generation. When our low rate constant value for k_7 is combined with known thermal rate constant values[11−14] of forward reaction *a* (k_{-7}) for the "third law" determination of $\Delta_f H°(C_2H_5)$, it agrees well with currently accepted thermochemistry of the ethyl radical.[22] Although the VLPR study of the Cl/C_2H_6/HBr three-component system is quite labor consuming when all the system parameters are employed, we undertook this task to measure the temperature rate coefficients for the title reactions and to search for the possible source of fundamental disparities between experimental techniques.

Experimental Section

The VLPR system used for current measurements at different temperatures is the same three-stage, all-turbo-pumped system in which the 298 K investigations were carried out.[22] It has been described in a series of our kinetic studies.[24−26] However, the temperature control, system parameters, experimental sequence, and data handling are briefly summarized in the following.

The thin-Teflon-coated cylindrical reactor cell of $V_r = 217.5$ cm^3 has a heating/cooling glass jacket connected to a thermostat bath circulator. A HAAKE FS2 type circulator was used at 333 and 368 K, but it was replaced by a Neslab ULT-80DD refrigerated bath circulator for the 265 and 228 K runs. Two thermocouples are mounted in the heating/cooling jacket, one at the bottom, the other at the top of the reactor cell, and the circulation speed of the bath fluid is adjusted to eliminate any measurable temperature difference between the two thermocouples. A heat-insulating cover is also applied to the outer surface of the reactor jacket to assist the uniform temperature setting and to protect the glass surface from ice deposition at low temperatures. This keeps the reactor temperature within ±0.1 °C over the entire temperature range.

The reactor cell operates in the Knudsen flow regime. The reactor base is sealed to a Teflon-coated, rapidly adjustable slide mechanism[24] having three interchangeable escape orifices with diameters of 0.193, 0.277, and 0.485 cm. They change the gas escape unimolecular rate, k_{eM}, which permits the variation of the reactor residence time by a factor of 5 in three steps. The use of these orifice sizes in different experimental runs is indicated as ϕ_2, ϕ_3, ϕ_5, respectively, in Tables 1 and 2, and are marked with different symbols in Figures 2 and 3. With our reactor volume V_r, the first-order escape rate constant for any gas component of mass M is given by $k_{eM} = a_\phi(T/M)^{1/2}$ s^{-1}, where T is the absolute temperature and $a_\phi = 0.258$ for ϕ_2, 0.546 for ϕ_3, and 1.321 for ϕ_5 orifices.[24] All escape rate constants appearing in eqs 1−6 were calculated with the above formula at different temperatures.

The reactor discharge is an effusive molecular beam through the selected exit orifice. The beam is chopped by a tuning fork chopper and further collimated by two pinholes at the entrances of two successive, differentially pumped chambers to reduce the background mass signals. This beam is sampled with the off-axis mass analyzer of a BALZERS QMG 511 quadrupole mass spectrometer. Its mass signal is fed to a phase sensitive lock-in amplifier tuned to the chopping frequency. Mass ranges of kinetic interest are repeatedly scanned, usually 20−30 times to give a good statistical average, and the mass intensities are recorded for data acquisition. Each mass signal is corrected for its small background value recorded prior to start-up of reaction and remeasured at the end.

Gas inlets are affixed on the top of the reactor cell for separate inlet flows of reactants. They are preceded by resistive capillary flow subsystems calibrated for regulating the fluxes of initial gas components[24] with the use of Validyne transducers. The flow of a Cl_2/He mixture traverses a phosphoric acid coated quartz discharge tube centered in the Opthos microwave generator cavity of a McCarrol antenna before joining at the tapered capillary inlet of the reactor cell. This strictly controlled gas inlet and outlet dynamics establish the well-defined steady state conditions in the reactor. Back-diffusion from the reactor to upstream gases is prevented by the use of very small conductance inlet capillaries relative to the conductance of the exit apertures.

In typical operation, the chlorine flow is started first using a 4.5% Cl_2/He gas mixture (both are Matheson research-grade gases), and the signal intensities of Cl_2 mass isotopes are repeatedly scanned using 20 V electron energy in the mass range of $m/e = 70-74$ for checking the instrumental reproducibility

TABLE 1: Initial and Steady State Concentrations[a] of Reactants and Ethyl Radical Formed before Introducing HBr into the System

no./ϕ_x	$I°_{Cl}/I°_{Cl} + I°_{HCl} \times 10^2$	$[Cl]_0$	$[C_2H_6]_0$	$I°_{Cl}/I°_{Cl} + I_{HCl} \times 10^2$	[Cl]	$[C_2H_6]$	$[C_2H_5]$	$\sum P_i$[b]
				$T = 368$ K				
$1/\phi_5$	52.72	3.50	4.17	11.04	0.732	2.11	1.62	0.26
$2/\phi_5$	52.52	4.10	5.33	9.20	0.718	2.70	2.09	0.31
$3/\phi_5$	53.55	4.85	5.92	8.75	0.792	2.92	2.29	0.35
$4/\phi_3$	51.21	12.02	9.42	3.80	0.892	2.64	3.49	0.70
$5/\phi_3$	48.75	10.67	8.78	3.63	0.794	2.67	3.29	0.65
$6/\phi_3$	50.66	9.55	7.85	4.19	0.790	2.38	2.99	0.57
$7/\phi_2$	45.75	19.23	11.19	2.31	0.971	1.81	3.30	1.06
$8/\phi_2$	48.06	21.90	13.36	2.10	0.946	2.25	3.80	1.18
				$T = 333$ K				
$1/\phi_5$	54.28	4.45	5.92	8.35	0.685	3.06	2.21	0.30
$2/\phi_5$	54.89	4.86	6.42	8.05	0.712	3.29	2.39	0.32
$3/\phi_3$	45.89	7.73	7.93	3.02	0.509	3.17	2.87	0.49
$4/\phi_3$	40.91	8.11	8.90	2.27	0.450	3.87	3.03	0.56
$5/\phi_3$	39.12	8.37	9.91	1.85	0.396	4.66	3.13	0.62
$6/\phi_2$	41.15	18.18	11.76	1.68	0.742	2.46	3.63	1.01
				$T = 265$ K				
$1/\phi_5$	57.64	4.89	7.13	7.18	0.610	3.83	2.44	0.27
$2/\phi_5$	58.66	5.39	7.51	6.90	0.634	3.98	2.55	0.29
$3/\phi_3$	59.11	13.32	10.91	3.53	0.785	3.20	3.70	0.52
$4/\phi_3$	49.37	11.84	11.30	2.40	0.576	4.12	3.71	0.55
$5/\phi_3$	50.23	13.95	10.15	2.96	0.765	3.02	3.47	0.52
				$T = 228$ K				
$1/\phi_5$	69.03	6.32	7. 56	8.74	0.800	3.55	2.79	0.25
$2/\phi_3$	52.67	10.72	8. 83	3.64	0.741	2.65	3.07	0.39
$3/\phi_3$	47.65	13.64	10. 75	2.37	0.569	3.94	3.51	0.46
$4/\phi_3$	62.82	13.90	10. 36	4.31	0.954	2.59	3.48	0.44
$5/\phi_2$	51.32	23.61	14. 89	1.91	0.877	2.50	3.73	0.77
$6/\phi_2$	51.16	27.31	16. 26	2.05	1.094	2.23	3.83	0.88

[a] All concentrations are in units of 10^{11} particles/cm^3.

of mass spectral efficiency α_{Cl2}. Then the microwave generator is turned on and its power is adjusted to 100% dissociation of Cl_2, controlled by observing the complete disappearance of Cl_2 mass signals. They are replaced with Cl atom and HCl signals in the mass range 35−38. HCl is produced in Cl atom reaction with H_3PO_4 wall coating of the discharge tube. It may constitute 35−60% of the overall Cl content (see column 2 of Table 1), but it is constant during an experimental run. After the Cl and HCl signals have reached steady values, the mass range 35−38 is repeatedly scanned using 20 eV to record the mass signal intensities of Cl atom isotopes at $m/e = 35$ and 37 and those of HCl at $m/e = 36$ and 38.

Next, the flow of ethane is started using 5% C_2H_6/He mixture (both are Matheson research-grade gases), and its flow rate is increased gradually until the mass 35 Cl signal drops to 0.2−0.04 of its original value. The mass range of 35−38 is scanned again to record the new signal intensities of Cl and HCl with 20 eV mass spectrometry. The mass range 25−30 is also scanned to record C_2H_6 and C_2H_5 signals and the distribution of their fragments using 20 eV first and then the more sensitive 40 eV mass spectrometry.

As a last step, the flow of pure HBr (Matheson 99.8% purity, further purified by trap-to-trap vacuum distillation) is started and increased gradually until some increase of mass signal 30 (and some decrease in mass signal 29) is observed. Mass ranges of 35−38, 25−30, and 79−82 are scanned to record the mass signal intensities for the calculation of Cl/HCl, C_2H_6/C_2H_5, and Br/HBr distributions, respectively, in this three-component reaction system using 20 eV mass spectrometry. Then the mass ranges of 25−30 and 79−82 are also scanned using the more sensitive 40 V electron energy.

Mass ranges of 114−118 and 158−162 were also checked regularly for possible traces of BrCl and Br_2 side reaction products of surface recombination. No detectable signal increase of these masses over the background values was ever found.

Treatment of Data and Results

The measured mass signal intensity, after corrections for its background signal and fragmentation, is proportional to the steady state concentration of a given substance in the reactor. This strictly linear proportionality is established by measuring the given mass signal intensity (I_M) as a function of the specific flux F(M) according to the relationship: $I_M = \alpha_M F(M)$, where α_M is the mass spectral sensitivity for an ion peak of mass M and $F(M) = (\text{flux})/V_r$ in molecule/(cm^3 s) units. The steady state concentration of the gas component M can then be calculated from the relation: $[M] = F(M)/k_{eM}$, molecule/cm^3. These formulas are universally applied to convert the measured mass signal intensities of Cl, HCl, C_2H_6, Br, and HBr into concentrations given in Tables 1 and 2.

Our mass analyzer is quite sensitive for the specific flux of each component in the range used. In absolute values they are $\alpha_{Cl} = \alpha_{HCl} = (2.69 \pm 0.06) \times 10^{-11}$, $\alpha_{RH} = (1.24 \pm 0.03) \times 10^{-11}$ at the parent mass intensity, where index RH stands for C_2H_6, and $\alpha_{HBr} = (8.13 \pm 0.18) \times 10^{-11}$, all with 20 eV mass spectrometry. Using 40 V electron energy the last two are $\alpha_{RH} = (3.91 \pm 0.04) \times 10^{-11}$ and $\alpha_{HBr} = (2.41 \pm 0.02) \times 10^{-10}$. The stability of F(M) depends on the upstream pressure reading which is done with ±0.1 Torr accuracy. Its error contribution is included in the scatter of α_M values. Such precision permits accurate measurements in flow rate changes with very small fluctuations. The application of these α_M values to our complex system is shown below.

It is found experimentally that $I_{Cl} + I_{HCl} =$ constant within ±2%. This allows the calculation of Cl/HCl distributions given in columns 2 and 5 of Table 1 and in column 3 of Table 2.

TABLE 2: Steady State Concentrations[a] of Reactants after Introducing the Initial Concentration of $[HBr]_0$ into the Cl + C_2H_6 Reaction System

no./$ø_x$	$[HBr]_0 \times 10^{-12}$	$I°_{Cl}/I°_{Cl} + I°_{HCl} \times 10^2$	$[Cl] \times 10^{-11}$	$[C_2H_6] \times 10^{-11}$	$[C_2H_5] \times 10^{-11}$	$I_{Br}/I_{Br} + I_{HBr} \times 10^2$	$[HBr] \times 10^{-12}$	$[Br] \times 10^{-11}$	$\sum P_i$[b]
				$T = 368$ K					
1/$ø_5$	0.80	4.53	0.300	3.02	0.906	6.92 ± 0.14	0.74	0.55	0.29
1a/$ø_5$	1.45	3.95	0.262	3.17	0.737	6.37 ± 0.14	1.36	0.92	0.31
2/$ø_5$	1.65	3.51	0.274	4.05	0.908	6.55 ± 0.26	1.54	1.07	0.37
2a/$ø_5$	2.79	2.90	0.226	4.30	0.650	5.47 ± 0.11	2.64	1.52	0.41
3/$ø_5$	4.22	3.00	0.272	4.64	0.712	6.52 ± 0.08	3.94	2.73	0.51
3a/$ø_5$	5.57	2.29	0.203	5.01	0.504	5.40 ± 0.18	5.27	2.97	0.56
4/$ø_3$	8.04	0.50	0.118	7.60	0.404	6.70 ± 0.35	7.50	5.35	1.00
5/$ø_3$	4.73	0.94	0.205	5.95	0.714	9.28 ± 0.16	4.29	4.36	0.83
5a/$ø_3$	6.43	0.80	0.175	6.33	0.525	8.70 ± 0.05	5.87	5.56	0.89
6/$ø_3$	6.74	1.08	0.203	5.34	0.474	9.80 ± 0.34	6.08	6.56	0.83
6a/$ø_3$	9.45	0.73	0.138	6.08	0.315	7.66 ± 0.24	8.73	7.19	0.93
7/$ø_2$	3.07	1.65	0.694	2.26	0.715	27.89 ± 0.77	2.21	8.50	1.18
7a/$ø_2$	4.73	1.11	0.467	3.20	0.518	24.10 ± 0.40	3.59	11.33	1.24
8/$ø_2$	4.37	1.14	0.514	3.58	0.698	23.41 ± 0.87	3.35	10.17	1.35
8a/$ø_2$	6.74	0.91	0.410	4.09	0.461	22.73 ± 0.05	5.21	15.22	1.44
				$T = 333$ K					
1/$ø_5$	1.63	3.84	0.315	4.29	1.129	6.68 ± 0.24	1.52	1.08	0.36
1a/$ø_5$	2.80	3.00	0.246	4.66	0.812	5.75 ± 0.10	2.64	1.60	0.40
2/$ø_5$	4.11	3.18	0.282	4.94	0.801	6.31 ± 0.19	3.85	2.58	0.47
2a/$ø_5$	5.48	2.55	0.226	5.24	0.617	5.37 ± 0.13	5.19	2.93	0.51
3/$ø_3$	4.18	2.06	0.347	4.32	0.763	12.43 ± 0.35	3.66	5.16	0.63
3a/$ø_3$	6.14	1.38	0.233	5.08	0.546	10.02 ± 0.27	5.52	6.11	0.70
4/$ø_3$	7.08	1.11	0.220	5.74	0.507	9.07 ± 0.11	6.44	6.39	0.81
4a/$ø_3$	9.94	0.64	0.127	7.13	0.391	7.30 ± 0.15	9.21	7.21	0.90
5/$ø_3$	8.45	0.82	0.175	6.87	0.541	8.18 ± 0.32	7.76	6.87	0.91
5a/$ø_3$	12.81	0.65	0.140	7.67	0.325	7.41 ± 0.23	11.86	9.43	1.06
6/$ø_2$	2.92	1.30	0.576	2.87	0.969	20.65 ± 0.42	2.32	5.99	1.11
6a/$ø_2$	4.59	0.79	0.350	4.39	0.684	16.81 ± 0.31	3.82	7.68	1.17
				$T = 265$ K					
1/$ø_5$	1.94	5.26	0.447	4.49	1.573	7.05 ± 0.18	1.80	1.36	0.32
1a/$ø_5$	3.60	4.40	0.376	4.94	1.124	6.54 ± 0.07	3.36	2.34	0.37
2/$ø_5$	4.26	5.34	0.491	4.75	1.210	7.87 ± 0.07	3.92	3.33	0.40
2a/$ø_5$	5.74	5.27	0.485	4.73	1.095	8.24 ± 0.06	5.27	4.70	0.44
3/$ø_3$	3.62	2.96	0.658	3.71	1.311	14.20 ± 0.15	3.10	5.10	0.62
3a/$ø_3$	6.54	1.73	0.384	5.27	0.817	11.21 ± 0.22	5.81	7.29	0.70
4/$ø_3$	8.69	1.47	0.353	5.71	0.649	11.15 ± 0.54	7.72	9.63	0.79
4a/$ø_3$	12.02	0.94	0.225	7.22	0.458	8.56 ± 0.26	10.99	10.22	0.88
5/$ø_3$	10.71	1.12	0.290	5.86	0.527	8.54 ± 0.31	9.79	9.09	0.82
5a/$ø_3$	12.93	0.84	0.217	6.69	0.421	7.21 ± 0.29	11.10	9.26	0.88
				$T = 228$ K					
1/$ø_5$	2.92	8.20	0.751	3.86	1.696	8.62 ± 0.08	2.67	2.50	0.32
1a/$ø_5$	4.59	5.76	0.527	4.61	1.277	6.98 ± 0.09	4.27	3.18	0.36
2/$ø_3$	3.69	3.50	0.712	2.76	1.052	13.95 ± 0.37	3.17	5.11	0.48
2a/$ø_3$	6.35	2.39	0.487	3.62	0.697	11.92 ± 0.13	5.59	7.52	0.54
3/$ø_3$	10.21	0.97	0.233	6.74	0.553	7.38 ± 0.35	9.46	7.49	0.71
3a/$ø_3$	14.96	0.79	0.190	7.34	0.375	6.71 ± 0.21	13.96	9.97	0.82
4/$ø_3$	12.01	2.15	0.476	4.29	0.434	13.23 ± 0.21	10.42	15.78	0.72
5/$ø_2$	3.90	1.52	0.699	2.87	0.952	17.28 ± 0.15	3.23	6.69	0.87
5a/$ø_2$	5.55	1.02	0.469	3.99	0.906	15.67 ± 0.75	4.68	8.64	0.90
6/$ø_2$	5.20	1.52	0.811	2.67	0.681	22.33 ± 0.17	4.04	11.53	1.00
6a/$ø_2$	8.56	0.80	0.430	4.66	0.420	15.68 ± 0.45	7.22	13.34	1.08

[a] All concentrations are in units of particles/cm.3 For data at 298 K see ref 22. [b] $\sum P_i$ is the total pressure in mTorr units of the system calculated from steady state concentrations of all species including HCl and He.

Since the HCl fragmentation into Cl^+ is only 0.24% at 20 V ionizing electron energy,[24,27] corrections are made when the Cl ratio drops below 6%. With total decomposition of Cl_2, the steady state Cl concentration can be calculated as $[Cl] = 2F(Cl_2)I_{Cl}/(I_{Cl} + I_{HCl})k_{eCl}$. These Cl concentration values are given in columns following the data entries of Cl/HCl distributions in Tables 1 and 2.

The mass spectrometry of C_2H_6 involves a complex mass fragmentation process[27] which reduces the α_{RH} value for the parent mass intensity measurement. Distributions of C_2H_6 mass fragments in the mass range of 25−30 are well studied in our system.[22,27] With the two ionizing electron energies used in our mass spectral analysis, they are in percentage

$$I°_{26}:I°_{27}:I°_{28}:I°_{29}:I°_{30} = 0.12:0.52:58.3:8.05:33.0$$

with 20 eV mass spectrometry, and

$$I°_{25}:I°_{26}:I°_{27}:I°_{28}:I°_{29}:I°_{30} = 0.36:7.72:15.4:48.7:11.8:16.1$$

with 40 eV mass spectrometry, where the subscripts of $I°_M$ denote the mass numbers of fragment signals and the upper index indicates that no chemical reaction is taking place in the system. The $I°_{30}$ ratio is directly proportional to $F(C_2H_6)_0$, that is $\alpha_{30} = \alpha_{RH}$, according to the relationship $0.161\sum I°_M = \alpha_{RH}F(RH)_0$ with 40 eV and $0.330\sum I°_M = \alpha'_{RH}F(RH)_0$ with 20 eV mass spectrometry. Of course, α_M values for mass fragments can also be calculated with the same type of relationships from which α_{29}, calculated as $8.05 \times 10^{-2}\sum I°_M/F(RH)_0 = \alpha'_{29}$ with 20 eV and $0.118\sum I°_M/F(RH)_0 = \alpha_{29}$ with 40 eV mass spectrometry, will be used for the derivation of the ethyl radical mass spectral sensitivity α_R.

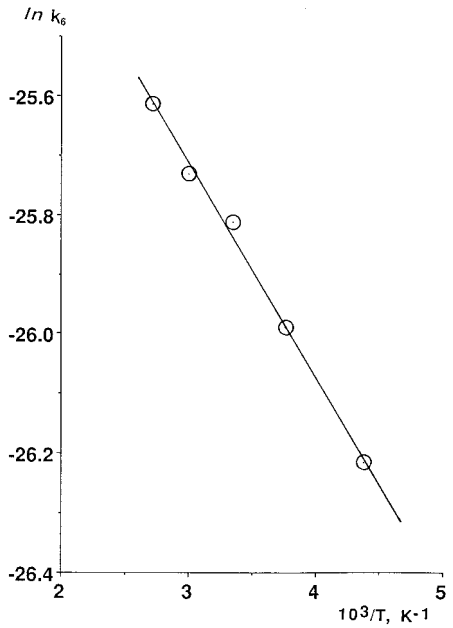

Figure 1. Arrhenius plot of rate constants of reaction 6.

In the Cl + C_2H_6 two-component system, the following elementary reactions are taking place in the millitorr pressure range given in the last column of Table 1:

$$Cl + C_2H_6 \xrightarrow{1} HCl + C_2H_5$$

$$Cl + C_2H_5 \xrightarrow{2} HCl + C_2H_4$$

$$2C_2H_5 \xrightarrow{3} C_2H_6 + C_2H_4$$

$$Cl + C_2H_4 \overset{4}{\rightleftharpoons} HCl + C_2H_3$$

$$Cl + C_2H_3 \xrightarrow{5} HCl + C_2H_2$$

This reaction system has been well explored and all rate constants involved, as well as their temperature dependencies, are known from our earlier work[25,27] using the same VLPR system.

When the ethane flow is introduced at rates corresponding to $[C_2H_6]_0$ concentrations given in column 4 of Table 1, the I°_{30} signal decreases to I_{30}, while the intensities of other lower mass number signals, especially those of I_{29} and I_{28}, increase. The new steady state concentration of ethane can be calculated as $[C_2H_6] = I_{30}/\alpha_{RH}k_{eRH}$ using both 20 and 40 eV mass spectral signal measurements. Since the concentrations calculated from the two electron voltage measurements are well within the statistical scatter of the I_{30} signal, the averages are given in column 7 of Table 1.

From the steady state kinetic equations of C_2H_6 and C_2H_5, the ethyl radical concentration can be derived[25] as

$$[R] = \frac{2\Delta[RH]k_{eRH} - k_1[RH][Cl]}{k_2[Cl] + k_{eR}} \qquad (1)$$

where $\Delta[RH] = [RH]_0 - [RH]$. Using the known rate constants[25] of $k_1 = (8.20 \pm 0.12) \times 10^{-11} \exp[-(170 \pm 20)/RT]$ and $k_2 = (1.20 \pm 0.08) \times 10^{-11}$ cm^3/(molecule s), as well as the tabulated concentrations of [RH] and [Cl] of Table 1, eq 1 can be solved for [R]. Their values are given in column 8 of Table 1. In turn, these ethyl radical concentrations are proportional to the excess in I_{29} signal intensities over the fragment signal contribution from RH; that is $\Delta I_{29} = I_{29} - I_{30}\alpha_{29}/\alpha_{RH}$,[28] and the mass spectral sensitivity of the ethyl radical can be obtained as $\alpha_R = \Delta I_{29}/[R]k_{eR}$. These α_R values averaged for all experimental runs of Table 1 are $\alpha_R(V_1{=}20\text{eV}) = (0.860 \pm 0.042) \times 10^{-11}$ and $\alpha_R(V_1{=}40\text{eV}) = (1.320 \pm 0.045) \times 10^{-11}$, about the same as we reported earlier.[25] Since they are derived from signal intensity differences, the scatter is about twice the scatter of α_M values for other substances.

We note that the data set of Table 1, besides providing $[Cl]_0$ and $[RH]_0$ concentrations, mainly serve for precise checking of our system operation and for the exact calibration of α_R for each run. Accurate ethyl radical concentration measurement depends on an accurate measurement of the parent mass signal intensity (I_{30}) for the ethane concentration. The most sensitive fragment signal I_{28} cannot be used for this purpose, as it is composed of contributions from fragmentations of RH and R, as well as of C_2H_4 product signal.

When pure HBr is introduced into the system with varied flow rates, which correspond to $[HBr]_0$ concentrations given in column 2 of Table 2, the Cl, C_2H_5, and HBr mass signal intensities decrease, while HCl, C_2H_6, and C_2H_4 signals increase, and Br signal appears in excess over the HBr fragmentation. These changes in mass signal intensities arise from the following new reactions:

$$Cl + HBr \xrightarrow{6} HCl + Br$$

$$C_2H_5 + HBr \xrightarrow{7} C_2H_6 + Br$$

$$Br + C_2H_5 \xrightarrow{8} HBr + C_2H_4$$

Usually two different $(HBr)_0$ flow rates are used for each Cl/C_2H_6 two-component runs. The second one is marked with "a" in the run numbering in column 1 of Table 2.

The new Cl/HCl distributions and the Cl concentrations are calculated from the corresponding signal intensities in the same way as was done for the two-component case. These data are given in columns 3 and 4, respectively, of Table 2. Ethane and ethyl radical concentrations are calculated from the recorded I_{30} and the ΔI_{29} signal intensities using α_{RH} and α_R values determined in their preceding two-component run. These concentrations are listed in columns 5 and 6 of Table 2.

Mass fragmentation of HBr was investigated[29] as a function of applied electron voltages between 17 and 65 eV. At the two electron voltages used in the present mass spectral analysis, the HBr fragmentation ratios[29] are $10^2 I_{79}/(I_{79} + I_{80}) = 0.30 \pm 0.08$ with 20 eV and 25.64 ± 0.19 with 40 eV electron energies, and they are the same for the 81/82 isotope mass combination. Correcting the measured mass signal intensities of mass range 79−82 for the above fragmentation ratios, the steady state distribution of Br/HBr due to reactions 6−8 can be calculated. With two isotope compositions (^{79}Br and ^{81}Br) and with two different electron energy measurements, four Br/HBr distribution data are obtained for each run. Their average is given in column 7 of Table 2. With the known inlet flow rate of HBr, the steady state concentration of Br atom can be obtained as $[Br] = F(HBr)_0 I_{Br}/(I_{Br} + I_{HBr})k_{eBr}$ (column 9 of Table 2), while the use of the complementary distribution factor with k_{eHBr} gives the steady state HBr concentration (column 8 of Table 2).

Data of Table 2, together with $[Cl]_0$ and $[C_2H_6]_0$ values of Table 1, provide the detailed numerical data base for kinetic calculations. All three initial components and the reactor

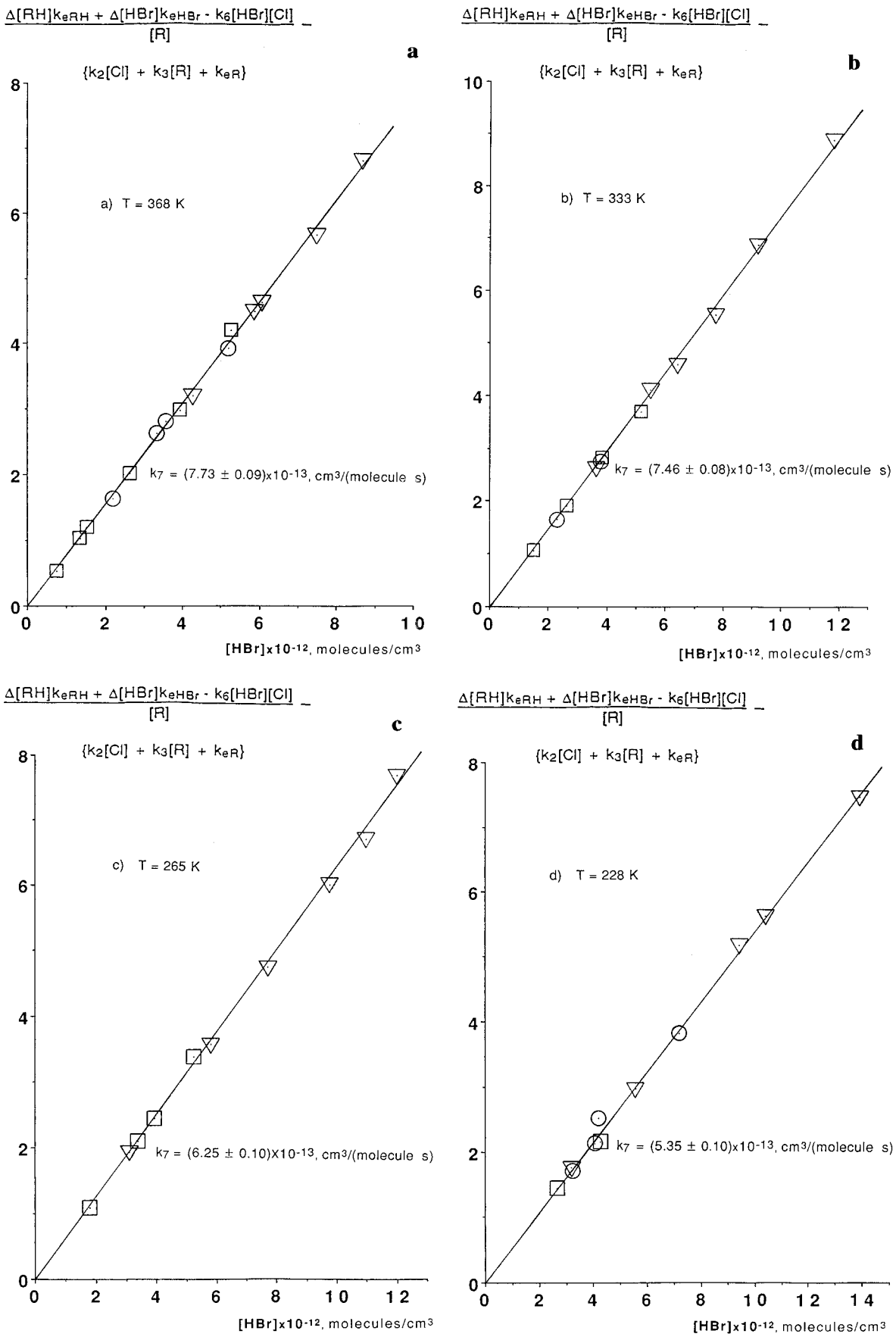

Figure 2. Dependence of HBr consumption and formation rates on the steady state concentration of HBr according to eq 3 at different temperatures. Slopes give k_7 directly. Symbols indicating the orifices used for given data pairs: ⊙, ϕ2; ⟁, ϕ3; ⊡, ϕ5.

residence time (escape orifice size change) are varied to accomplish a multiparametric kinetic study. The overall HBr consumption is varied between 5.5 and 27.9%, and it is measured to ±2.5%.

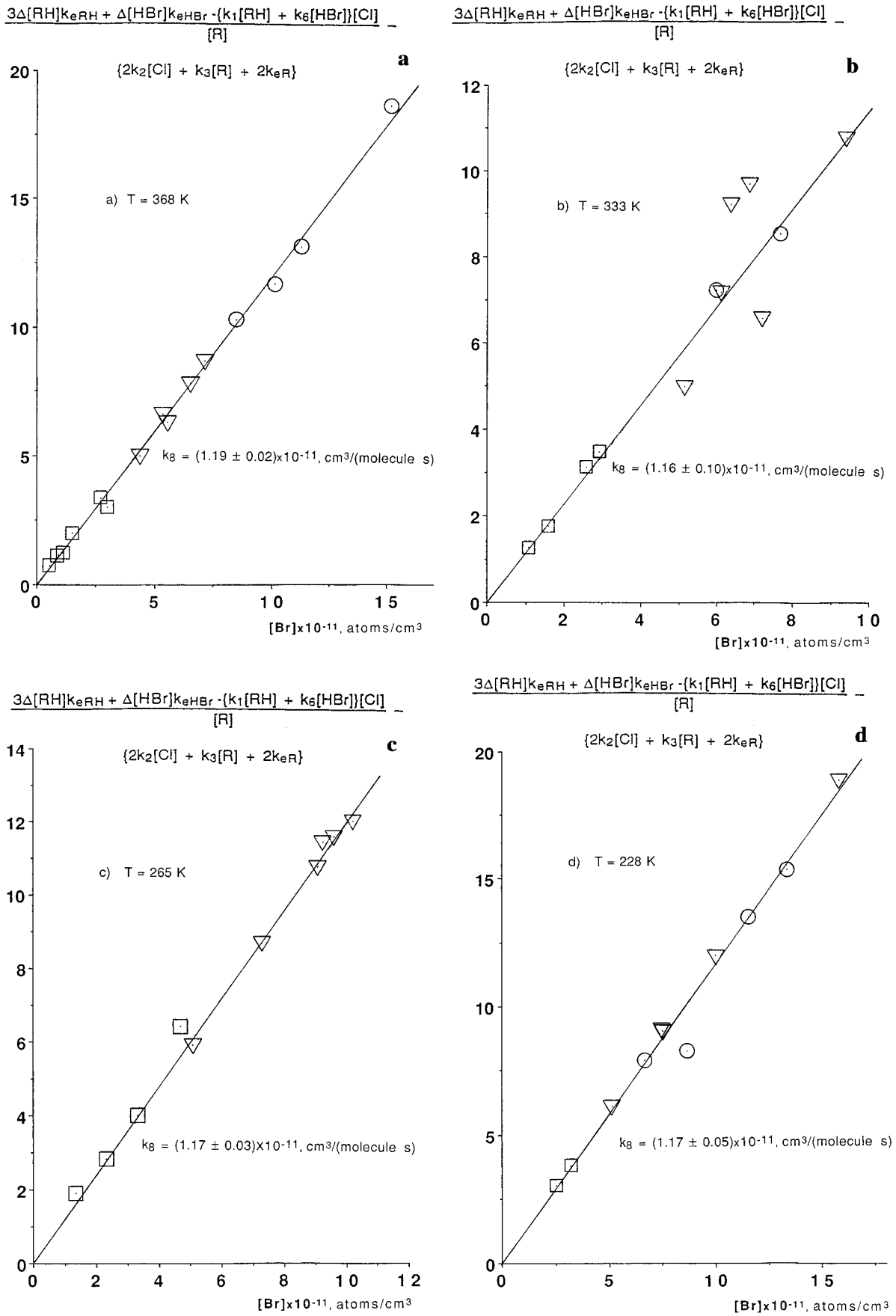

Figure 3. Dependence of Br atom formation and consumption rates on the steady state concentration of Br according to eq 4 at different temperatures. The slope gives k_8 directly. Symbols of orifices are the same as in Figure 2.

Combinations of steady state equations derived for each substance in the reaction system lead to algebraic equations that are first order in all rate constants. They may also be solved for the ethyl radical concentration and for the HBr mass balance in an explicit way. Detailed steady state algebraic treatment of this multicomponent kinetic system is given in our preceeding

paper.[22] The derived equations are

for the ethyl radical steady state concentration:

$$[R] = \frac{2\Delta[RH]k_{eRH} - k_1[RH][Cl]}{k_2[Cl] - k_7[HBr] + k_8[Br] + k_{eR}} \quad (2)$$

where [R] is measured directly (column 6 of Table 2),

for HBr consumption kinetics:

$$k_7[HBr] = \frac{\Delta[RH]k_{eRH} + \Delta[HBr]k_{eHBr} - k_6[HBr][Cl]}{[R]} - \{k_2[Cl] + k_3[R] + k_{eR}\} \quad (3)$$

for Br atom kinetics:

$$k_8[Br] = \frac{3\Delta[RH]k_{eRH} + \Delta[HBr]k_{eHBr} - \{k_1[RH] + k_6[HBr]\}[Cl]}{[R]} - \{2k_2[Cl] + k_3[R] + 2k_{eR}\} \quad (4)$$

for the mass balance of HBr conversion:

$$\Delta[HBr]k_{eHBr} = [Br]k_{eBr} \quad (5)$$

where $\Delta[RH]$ and $\Delta[HBr]$ represent the difference between the initial $[RH]_0$ or $[HBr]_0$ and the steady state concentration of [RH] or [HBr], respectively. The last two are measured in the three-component system (Table 2).

Equations 2−5 are all exact, derived directly from the steady state condition.

Equations 3 and 4 are of primary interest for obtaining rate constants k_7 and k_8. For their solution, all concentrations involved are measured and given in Tables 1 and 2. For k_1 and k_2 values are given above in connection with eq 1, and $k_3 = (2.00 \pm 0.06) \times 10^{-12}$ cm^3/(molecule s) is taken from our earlier VLPR study[25] of Cl + C_2H_6 reaction. k_6 comes from our recent study[30] of reaction 6 in the same system.

The kinetics of reaction 6 was investigated in parallel with the present work using the Cl/HBr two-component variant. It is a simple kinetic system where only the single reaction Cl + HBr takes place, leading to the steady state equation for both the Cl atom consumption and the Br atom formation rates as

$$\frac{\Delta[Cl]}{[Cl]}k_{eCl} = \frac{[Br]}{[Cl]}k_{eBr} = k_6[HBr] \quad (6)$$

Measurements of both rates were carried out simultaneously in the same temperature range with the same temperature steps as the present study. The Arrhenius plot of measured k_6 values is presented in Figure 1. The linear fit of these data corresponds to the Arrhenius equation

$$k_6 = (1.99 \pm 0.10) \times 10^{-11} \exp[-(710 \pm 29)/RT] \text{ cm}^3/(\text{molecule s})$$

which is in good agreement with the results obtained by laser flash time-resolved Cl atom fluorescence measurements.[31]

Having all the necessary input data, eq 3 can be solved for k_7 at each temperature run. Plots of the left side of eq 3 vs [HBr] are presented in Figure 2a−d for four different temperature measurements, where the slopes give the rate constants of reaction 7 directly. Their values obtained with linear regression are shown in each part of the figure.

Reaction 6 is about 10 times faster than reaction 7. Even at low Cl concentration its rate is still high enough to produce Br atoms in considerable concentrations. Thus the rate of reaction 8 becomes comparable with that of reaction 7 in competition for ethyl radical consumption with a significant feedback of HBr. It can be evaluated by solving eq 4 for k_8 in a way similar to the solution of eq 3. Plots of the left side of eq 4 vs [Br] are presented in Figure 3a−d for four different temperature measurements, where the slopes give the rate constants k_8 directly. Their values calculated with linear regression are shown in each part of the figure.

All eight linear plots in Figures 2 and 3 have zero intercepts, and all data of different residence times fit well on each straight line. This indicates the absence of any side reaction outside the given mechanism. If there were any wall loss of atoms or radicals, it would have introduced nonzero intercepts and produced different k values with the data taken using different residence times. With the reactor surface area of 222 cm^2, depending on the escape orifice size used, wall collisions are generally 10^2 to 10^3 times more frequent than reactive collisions in the reactor cell. But the reactor surface is made inert by the thin Teflon coating. That is why we have excellent mass balances for Cl and HCl, as well as for Br and HBr, under all reaction conditions at pressures given in the last columns of Tables 1 and 2. It is not surprising, since the Teflon surface has a very low sticking coefficient (γ = reaction/wall collision) for Cl atom,[32] $\gamma_{Cl} = 5 \times 10^{-6}$, and for Br atom,[33] $\gamma_{Br} = 5.3 \times 10^{-5}$. These would contribute negligibly to wall removal of X atoms compared to the escape rate constant k_{eX}.

With the knowledge of k_7 and k_8, the ethyl radical concentration in the three-component system can now be calculated according to eq 2 and checked against the radical concentrations measured directly for each run. This comparison is presented in Figure 4, where the data for the abscissa are taken from column 6 of Table 2. Independent of the temperature and residence time (orifice size) variations, measured $[C_2H_5]$ values are in excellent conformity with calculated ethyl radical concentrations, resulting in a slope of 1.01 ± 0.03. This test of the entire mechanism indicates that the experimental recovery of ethyl radical is established within 3% accuracy, leaving no room for significant wall removal of radicals.

The observed values of k_7 show normal behavior, increasing with increasing temperature. This is presented as an Arrhenius plot in Figure 5 with circles. The straight line fitted to these data is represented by the Arrhenius equation

$$k_7 = (1.43 \pm 0.06) \times 10^{-12} \exp[-(444 \pm 26)/RT] \text{ cm}^3/(\text{molecule s})$$

The precision of both the *A*-factor and the activation energy is around 5%, which is consistent with the low scatter of rate constant measurements (∼1.5%) at each temperature. The reported results of Seakins *et al.*[7] (hexagons with full line) and Nicovich *et al.*[23] (squares with broken line) are also shown in Figure 5. The disagreement with our results is striking.

Discussion

Rate constant k_8 shows no temperature dependence which would exceed the scatter of measurements. The average of five different temperature measurements, between 368 and 228 K, including the value reported earlier[22] for 298 K, gives

$$k_8 = (1.18 \pm 0.05) \times 10^{-11} \text{ cm}^3/(\text{molecule s})$$

which is slightly less than k_2 of Cl + C_2H_5 reaction. Both

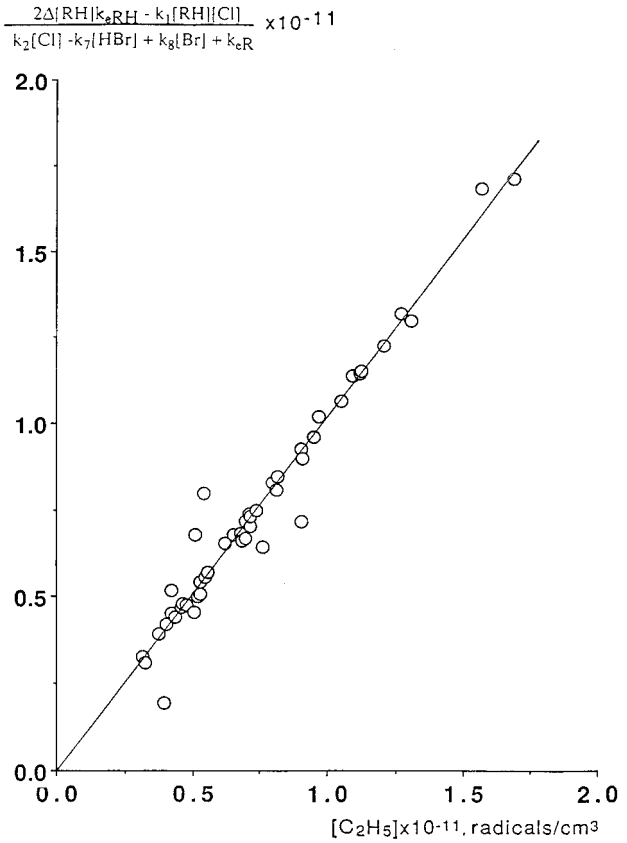

Figure 4. Comparison of ethyl radical concentrations calculated according to eq 2 with measured C_2H_5 concentrations given in column 6 of Table 2 (abscissa).

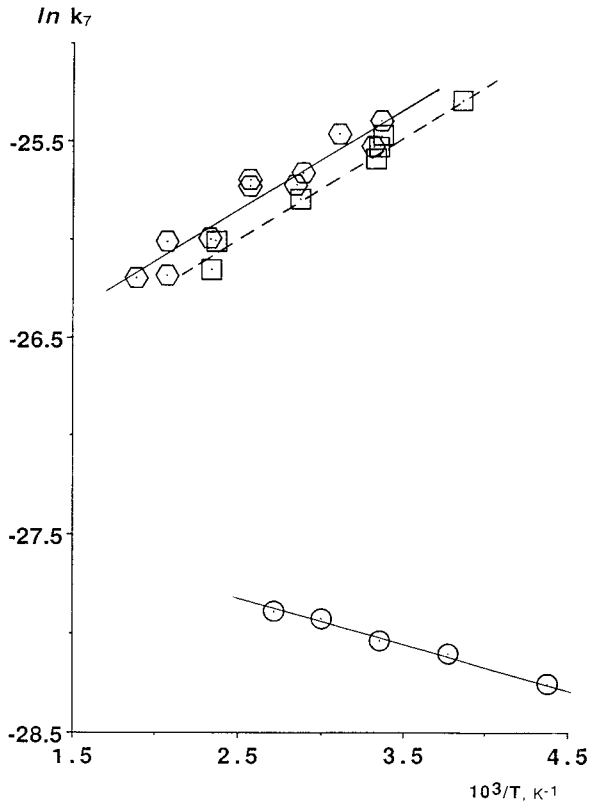

Figure 5. Arrhenius plot of rate constants k_7. Circles show present results taken from Figure 1a−d and the 298 K data from ref 22. Hexagons with solid line represent the data of ref 7. Squares with broken line display the data of ref 23.

reactions are interpreted as proceeding via a recombination to form an excited singlet $(C_2H_5X)^*$ molecule. Note that the singlet restriction reduces its rate of formation by a factor of 8 from collision frequencies. Its formation is followed by a rapid four-center elimination to produce HX. The average lifetime of the excited molecule is estimated to be $<10^{-7}$ s, which is about 300-fold shorter than the time elapse between collisions in our low-pressure reactor cell. This large time difference precludes the formation of any measurable atom + radical recombination product.

Our measured rate constant k_7 is about 14 times less at 298 K than those reported[7,23] by works with laser flash generation of ethyl radical. In order for our rate constant to be in error by a factor of 14, our value of steady-state C_2H_5 radical concentration would have to be 14 times smaller than we have reported. Since the steady state C_2H_5 radical concentration varies from 25 to 35% of total C_2 species, such a gross error would destroy the very good mass balances (3%) we have found (Figure 4) for the steady state C_2H_5 and C_2H_6 concentrations, the major C_2 species along with C_2H_4.

This gross discrepancy is mainly accounted for by the difference of activation energies as vividly presented in Figure 5, while the A_7-factors are roughly within the reported scatters (see Table 3). A similar situation can be found for the t-C_4H_9 + HI reaction[9,35] and for the comparison of the original (uncorrected) *ab initio* calculation[18] and experimental[9] data of CH_3 + HBr reaction. In both cases the A-factors show approximate agreements, but positive activation energies[18,35] in contrast with negative activation energies were reported[9] for both reactions.

It is of interest to see how the variations of measured negative or positive activation energies E_7 would affect the thermochemistry of reaction 7. Calculations are made using all available kinetic data for the forward (7) and reverse (−7) reactions to derive the enthalpy of reaction, $\Delta H°_7$, and the heat of formation of the ethyl radical $\Delta_f H°(C_2H_5)$.

Rate parameters known for the forward reaction 7 are summarized in Table 3. Since the measured rate constant values of Seakins *et al.*[7] and Nicovich *et al.*[23] have a reasonable overlap in their common temperature range (Figure 5), we put their data into one unified Arrhenius function (line 3a of Table 3), which resulted in lower scatter for both the A-factor and the activation energy.

Similarly, the known rate parameters for the reverse reaction (−7) are collected in Table 4. There is one earlier study[36] on the direct photobromination of ethane in the 308−363 K temperature range from which only the activation energy E_{-7} = 13.6 ± 0.5 kcal/mol could be extracted. Its inclusion into the second law thermochemical calculation would give $\Delta_f H°_7$ indistinguishable from those obtained from E_{-7} of lines 3b and 4b (Table 4). We note that the uncertainty in E_{-7} in line 1b exceeds our measured activation energy E_7 (line 4a of Table 3), while all the rest are about half of that. Since our experimental investigation of k_7 has no temperature overlap with temperature ranges of the reverse reaction studies, k_{-7} at 298 K is calculated outside the experimental temperature range using the modified Arrhenius equation[37]

$$k_{-7} = A'_{-7}(T_m/298)^n \exp(-E'_{-7}/RT) \qquad (7)$$

where $E'_{-7} = E_{-7} - nRT_m$ and $A'_{-7} = A_{Tm}\,(T_m/298)^{-n}$. T_m is the mean temperature of experimental measurements calculated from the $1/T$ function and A_{tm} is the A-factor at T_m temperature calculated from the two-parametric Arrhenius equation using E'_{-7}. They are given in columns 5−7 of Table 4. $n = \langle \Delta Cp^{\ddagger} \rangle / R$ = 1.5 since $\langle \Delta Cp^{\ddagger} \rangle$ = 3.0 cal/(mol K) calculated with a tight transition state model.[22]

TABLE 3: Rate Parameter of Forward Reaction 7

no.	temperature range [K]	$A_7 \times 10^{12}$ [cm^3/(molecules s]	E_7 [cal/mol]	$k_7(298) \times 10^{13}$ [cm^3/(molecule s)]	$k_7(530) \times 10^{12}$ [cm^3/(molecules)]	ref and notes
1a	297−530	1.70 ± 0.55	−1000 ± 278	91.63 ± 29.65	4.38 ± 1.42	7
2a	259−427	1.33 ± 0.33	−1078 ± 156	81.20 ± 20.15		23
3a	259−530	1.69 ± 0.20	−969 ± 82	85.90 ± 10.17	4.22 ± 0.50	average: 1a,2a
4a	228−368	1.43 ± 0.06	444 ± 26	6.79 ± 0.28	1.20 ± 0.05[a]	this work

[a] Calculated using the modified Arrhenius equation 7 fitted to $T_m = 282$ K with $A^1{}_7 = 3.47 \times 10^{13}$ cm^3 (molecule s) and $E^1{}_7 = -402$ cal/mol.

TABLE 4: Rate Parameters of Reverse Reaction −7

no.	temperature range [K]	$A_{-7} \times 10^{10}$ [cm^3/(molecule s)]	E_{-7} [kcal/mol]	T_m [K]	$A'_{-7} \times 10^{11}$ [cm^3/(molecule s)]	E'_{-7} [kcal/mol]	$k_{-7}(298) \times 10^{20}$ [cm^3/(molecule s)]	ref
1b	473−621	2.35 ± 1.12	12.74 ± 0.50	537	2.17 ± 1.03	11.13 ± 0.50	16.89 ± 8.05	7
2b	494−592	6.61 ± 1.70	14.00 ± 0.24	539	6.12 ± 1.58	12.38 ± 0.24	5.80 ± 1.49	11
3b	332−472	1.23 ± 0.20	13.39 ± 0.27	390	1.83 ± 0.30	12.22 ± 0.27	2.27 ± 0.37	14
4b	312−483	2.26 ± 0.32	13.67 ± 0.14	379	3.52 ± 0.50	12.53 ± 0.14	2.59 ± 0.37	34
5b	308−363		13.6 ± 0.5	333				36

TABLE 5: $\Delta_f H°$ Ethyl Radical Calculated from Different Combinations of Equilibrium Reactions 7 and −7 at 298 K

combination no./no.	$K_7(298) \times 10^7$	$-\Delta H°_7$, 3rd law (kcal/mol)	$-\Delta_f H°(C_2H_5)$, 3rd law (kcal/mol)	$-\Delta H°_7$, 2nd law (kcal/mol)	$-\Delta_f H°(C_2H_5)$, 2nd law (kcal/mol)
3a/1b	5.09 ± 2.50	13.68 ± 0.49	29.10 ± 0.49	12.99 ± 0.51	28.39 ± 0.51
3a/2b	14.81 ± 4.19	14.31 ± 0.29	29.71 ± 0.29	14.25 ± 0.25	29.65 ± 0.25
3a/3b	37.84 ± 7.62	14.87 ± 0.23	30.27 ± 0.23	14.08 ± 0.28	29.48 ± 0.28
3a/4b	33.17 ± 6.15	14.79 ± 0.22	30.19 ± 0.22	14.40 ± 0.16	29.80 ± 0.16
4a/1b	0.40 ± 0.19	12.16 ± 0.47	27.56 ± 0.47	11.58 ± 0.50	26.98 ± 0.50
4a/2b	1.17 ± 0.31	12.80 ± 0.27	28.20 ± 0.27	12.84 ± 0.24	28.24 ± 0.24
4a/3b	2.99 ± 0.50	13.36 ± 0.21	28.76 ± 0.21	12.67 ± 0.27	28.07 ± 0.27
4a/4b	2.62 ± 0.39	13.28 ± 0.20	28.68 ± 0.20	12.99 ± 0.14	28.39 ± 0.14

A combination of data of Tables 3 and 4 is used for obtaining the standard enthalpy change of equilibrium 7 according to both the

third law: $\Delta H°_7 = 298(\Delta S°_7 - R \ln K_7)$

second law: $\Delta H°_7 = E_7 - E_{-7} - nR(298 - T_m)$

where $K_7 = k_7/k_{-7}$. $\Delta S°_7 = 10.4 \pm 0.5$ cal/(mol K), where the uncertainty arises from the entropy of the ethyl radical,[22] $S°(C_2H_5) = 59.6 \pm 0.5$ cal/(mol K). This contributes an extra ±0.15 kcal/mol uncertainty to the third law calculation of $\Delta H°_7$. $<\Delta Cp_7>$ is small and negligible[22] in the temperature range 298−600 K. From the reaction enthalpy change, the heat of ethyl radical formation is then calculated in the usual way,

$$\Delta_f H°(C_2H_5) = \Delta H°_7 - \Delta_f H°(HBr) + \Delta_f H°(Br) + \Delta_f H°(C_2H_6)$$

taking $\Delta_f H°$ values of HBr, Br, and C_2H_6 from JANAF tables.

All the details of the above calculations are summarized in Table 5, where the first column shows the sequence of data combinations taken from Tables 3 and 4. The first line of Table 5 gives $\Delta_f H°(C_2H_5) = 28.8 \pm 0.5$ kcal/mol for the average of the second and third law calculations, the same value as recommended by Berkovitz *et al.*[16] But the same average with the next three combinations from 3a/2b to 3a/4b results in $\Delta H°_7 = -14.45 \pm 0.30$ kcal/mol, and consequently in a higher value of $\Delta_f H°(C_2H_5) = 29.85 \pm 0.29$ kcal/mol, reflecting the negative activation energy used for the forward reaction 7. On the other hand, our measured rate parameters in the combination 4a/1b of Table 5 give the average of $\Delta_f H°(C_2H_5) = 27.3 \pm 0.5$ kcal/mol due to the lower activation energy E_{-7} in line 1b of Table 4. But the last three combinations from 4a/2b to 4a/4b give $\Delta H°_7 = -12.96 \pm 0.22$ kcal/mol and $\Delta_f H°(C_2H_5) = 28.40 \pm 0.25$ kcal/mol, which we recommend as our updated value for the heat of formation of ethyl radical obtained from chemical equilibrium study of reaction 7. It sets the bond dissociation enthalpy to $DH°(C_2H_5-H) = 100.5 \pm 0.3$ kcal/mol. It is in excellent agreement with results extracted from shock-tube decomposition of *n*-butane[4] and from the reversible thermal decomposition of ethyl radical[38] isolated from the high-temperature pyrolysis of ethane, where the first kinetic method corresponds to equilibrium *b*, while the second one to equilibrium *c* given in the Introduction. Both studies report the same value of $\Delta_f H°(C_2H_5) = 28.5 \pm 0.5$ kcal/mol. This *c* variant of the $H + C_2H_4 \rightleftharpoons C_2H_5$ equilibrium was also studied in a direct time-resolved system using 193 nm laser flash photodecomposition of C_2H_4 as an H atom source.[39] This system results in $\Delta_f H°(C_2H_5) = 28.4 \pm 0.4$ kcal/mol, or 28.7 ± 0.2 kcal/mol with high-pressure limiting adjustment for the forward reaction.[40]

The above survey indicates that the derived thermochemistry of ethyl radical using positive activation energies in both directions is in excellent agreement with the thermochemistry of bond fission and radical decomposition processes. This heat of formation of ethyl radical and bond dissociation energy of ethane are also in good agreement with the values suggested by Walker *et al.*[41] on the bases of general trends found in oxidation of *i*-C_3H_7 and *t*-C_4H_9 radicals, as well as with the value of Miyokawa *et al.*[17] derived from competitive photobromination results of ethane and monohalogenated ethane derivatives. The laser flash system[7] seems to fall in a separate class. Only the result of flash−flash combination (3a/1b of Table 5) is in line with present values where the reported negative activation energy for E_7 is compensated by a lower E_{-7} activation energy.

There are only two absolute rate measurements of reaction −7. One of them uses the experimental technique of laser flash photolysis of CF_2Br_2 for bromine atom source coupled with time-resolved resonance fluorescence measurement of Br atom depletion[7] upon reaction with ethane on about a 2−12 ms reaction time scale. The other uses the conventional thermal bromination of ethane.[11] They report different rate parameters,

TABLE 6: $\Delta_f H°(C_2H_5)$ Values of k_7 and k_{-7} at 530 K

combination no./no.	$K_7(530) \times 10^3$	$-\Delta H°_{7,}$ 3rd law (kcal/mol)	$-\Delta_f H°(C_2H_5)$, 3rd law (kcal/mol)	$-\Delta H°_7$, 2nd law (kcal/mol)	$-\Delta_f H°(C_2H_5)$, 2nd law (kcal/mol)
3a/1b	2.97 ± 1.47	14.04 ± 0.57	29.44 ± 0.57	14.37 ± 0.51	29.77 ± 0.51
3a/2b	3.43 ± 0.98	14.19 ± 0.35	29.59 ± 0.35	14.11 ± 0.25	29.51 ± 0.25
4a/1b	0.85 ± 0.40	12.71 ± 0.50	28.11 ± 0.50	12.83 ± 0.50	28.23 ± 0.50
4a/2b	0.98 ± 0.26	12.86 ± 0.28	28.26 ± 0.28	12.91 ± 0.24	28.31 ± 0.24

as shown in lines 1b and 2b, respectively, of Table 4. Over this temperature range, however, their absolute values agree to within 20%. At 530 K, $k_{-7} = (1.42 \pm 0.68) \times 10^{-15}$ of the flash system[7] and $(1.23 \pm 0.32) \times 10^{-15}$ cm^3/(molecule s) of the thermal system[11] differ by only 7.2%. Combining these values with forward rate constant data at 530 K given in Table 3, the obtained reaction enthalpies (corrected to 298 K using the very small $\langle \Delta Cp \rangle$ correction[22]) and heats of ethyl radical formation are summarized in Table 6. A comparison of data in Tables 5 and 6 indicates that while the combinations of 3a/2b and 4a/2b remain practically unchanged, the new high-temperature rate combinations of 3a/1b and 4a/1b in Table 6 are in complete agreement with their respective other (2b−4b) combinations in Table 5. It also reveals that only the calculation with 3a/1b combination given in Table 5 agrees with the enthalpy data reported by Seakins *et al*.,[7] where no combinations with other known back-reaction rates were made.

The disparity between the two absolute rate measurements[7,11] of reaction −7 is significant, as it can compensate for the negative activation energy measured[7] for the forward reaction 7. We note that the flash photolysis/Br atom resonance fluorescence system has no radical-scavenging process like the $R + Br_2$ reaction in the thermal system.[11] Therefore, $[Br]_0$ concentration must be kept low to avoid significant Br atom consumption in the fast reaction 8. From the ethane concentrations given in Table III of ref 7, we estimate that $[Br]_0$ should be kept below 2×10^{11} atom/cm^3 in the experimental runs. Another experimental problem is the diffusion loss of Br atoms out of the monitoring zone and its temperature dependence. According to the original report,[7] this diffusion is only a "minor loss term" of the Br atom removal; therefore no k_d data are provided in Table III of ref 7. However, if k_d is as high as measured directly (25 s^{-1} at 298 K) in the same experimental system,[42] it may constitute from 30 to 86% of the first order rate decay of Br atom fluorescence signal in the 473−621 K range. Inaccurate corrections might lead to higher rate constant values of k_{-7} and lower temperature dependence. No data for such details are reported,[7] but the marked concave curvature of the Arrhenius plot in Figure 2 of ref 7 indicates the influence of some side processes.

A comparison of the two absolute rate measurements[7,11] of reaction −7 is presented as Arrhenius plots of reported data in Figure 6a. The first four data of laser flash experiments[7] between 473 and 546 K give an Arrhenius function of $k_{-7} = (7.9 \pm 4.3) \times 10^{-10} \exp[-(13.99 \pm 0.80) \times 10^3/RT]$ cm^3/(molecule s). Although the *A*-factor is somewhat high, it is in fair agreement with the result of the thermal system[11] (compare with line 2b of Table 4). Rate constants of the upper temperature region[7] between 523 and 621 K can be described by an Arrhenius function of $k_{-7} = (0.60 \pm 0.20) \times 10^{-10} \exp[-(11.21 \pm 0.19 \times 10^3/RT$. Because of the high activation energy E_{-7}, the importance of the 2.78 kcal/mol energy change in the slope of Figure 6a is not very marked. Although both functions give the same $k_{-7} = 1.75 \times 10^{-15}$ cm^3/(molecule s) at $T_m = 537$ K, the rate constants at 298 K calculated using the modified forms of the above Arrhenius equations are different by a factor of 8. However, using what we called a reduced Arrhenius plot,[46] which emphasizes the experimental uncertainties in the form of

$$\ln[\Delta k_{-7}] = -\frac{(E_{-7} - 12)}{RT}103 + \ln A_{-7} \qquad (8)$$

presented in Figure 6b, the disparity becomes very clear. While the results of the conventional bromination kinetics[11] still retain a good linear Arrhenius relationship within the scatter, the laser flash bromination[7] results display a systematic error that breaks the Arrhenius function into two parts. The laser flash data represented by squares in Figure 6b would permit lines of any slope within the extremes of the two dashed lines shown to be drawn through them. Thus the experimental points of ref 7 could equally be represented by activation energies varying from 14 to 11.2 kcal/mol. Their *A*-factor would, of course, vary appropriately. This error justifies dropping the results of the 4a/1b combination from the 4a series in Table 5. It also shows that the agreement of the 3a/1b combination in Table 5 with our thermochemical results is accidental.

From the data of tables 5 and 6, it is seen that the difference in the heat of formation of ethyl radical between our derived value and that of Seakins *et al*.[7] is 1.4 kcal/mol, which is equal to the difference in activation energies E_7 given in Table 3. Our small positive activation energy is plausible on the basis of H atom metathesis. There is no explanation or precedent for a negative activation energy for what should be a direct metathesis reaction. In terms of H atom metathesis, it cannot be negative, and even the application of a contact transition state mechanism[43] (representing the highest rate for a bimolecular H atom transfer) would result in a rate constant k_7 that is about 1 order of magnitude less than reported by Seakins *et al*.[7] Some of our reservations concerning the techniques that have been employed have been discussed in earlier papers,[22,29,30] and we shall not consider them here.

Conclusion

The improved VLPR system is well suited for the measurement of temperature coefficients of the $C_2H_5 + HBr$ reaction 7 in the temperature range 228−368 K. This experimental system permits a broad kinetic investigation by allowing concentration variations of both reactants and of the reactor residence time. The simultaneous measurement of reactant consumptions and product formations gives an excellent mass balance for all species with ±3% accuracy. This is a powerful check for the overall reaction mechanism taking place in the VLPR system. Such a versatility is not provided by presently existing alternative techniques, which usually measure either the loss of a single reactant or the appearance of a single product in time, then fitting the obtained data to a proposed mechanism by making corrections for the observed extra radical loss such as the wall reaction of radicals[7] with no product identification in the laser flash/tube flow system or the unidentified "ghost" reaction[23] in the laser flash/Br atom fluorescence system.

Rate constants measured at different temperatures are well described by an Arrhenius equation, $k_7 = (1.43 \pm 0.06) \times 10^{-12} \exp[-(444 \pm 26)]/RT$ cm^3/(molecule s), where the small positive activation energy is in complete accordance with earlier as-

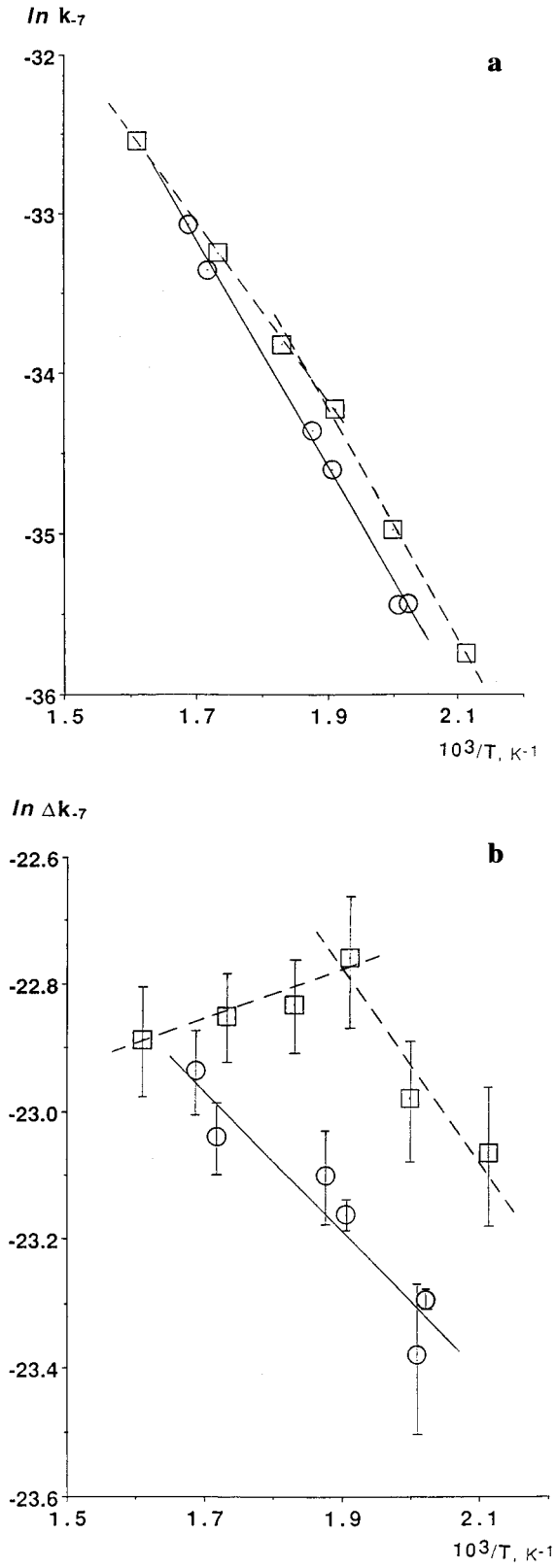

Figure 6. (a) Comparison of absolute rate measurements for reaction −7 presented as Arrhenius plots of reported data for conventional thermal bromination kinetics[11] (circles with full line) and laser flash bromination[7] (squares with broken lines) of ethane. (b) Reduced Arrhenius plot (eq 8) of data in part a. This type of plot gives better presentation of any systematic errors in *k*. While we have used two dashed lines to represent the data, a single line of arbitrary slope between zero and one parallel to the lower straight line would represent the upper points equally well.

sumptions[3] and with direct H atom metathesis. It disagrees with reported[7,23] negative activation energy of about −1 kcal/mol and with the proposed[10] mechanism of a two-step chemical activation process for H atom abstraction.

When our results are combined with all known kinetic data,[11,14,34] except with that of the laser flash bromination[7] of ethane, for the reverse reaction −7, the heat of ethyl radical formation deduced from both the second and third law is obtained as $\Delta_f H°(C_2H_5) = 28.40 \pm 0.25$ kcal/mol, which sets the bond dissociation enthalpy to $DH°(C_2H_5-H) = 100.5 \pm 0.3$ kcal/mol. These thermochemical values agree well with those obtained from high-temperature bond fission/radical recombination[4] and the reversible thermal decomposition[5,39] of the ethyl radical. The results of these three different chemical equilibria provide the currently accepted thermochemistry of the ethyl radical in a remarkable conformity.

The kinetic investigation of the laser flash bromination[7] of ethane involves a systematic error as disclosed in Figure 6a,b. Its low activation energy E_{-7} compensates for the the negative activation energy of the forward reaction, which leads to an apparent agreement with our thermochemical values. This agreement is actually an accidental outcome. All other combinations of reported kinetic data for the thermal bromination of ethane[11,14,34] with those of laser flash initiated reaction 7 give higher thermochemical values, reflecting the activation energy difference for reaction 7 between our value E_7 and those of Seakins *et al.*[7] and Nicovich *et al.*[23]

The general trend in the reported[7,9] negative activation energies for R + HX (or X_2) type reactions seems, we believe, to arise from some still undisclosed artifacts of the laser flash experimental system. We are of the opinion that this problem may arise from the energy sensitive cross section for near threshold photoionization of "hot" radicals[22] and their quenching by HBr and HI.

Rate constants obtained for the reaction 8 of C_2H_5 + Br show no measurable temperature dependence. Their average gives $k_8 = (1.18 \pm 0.05) \times 10^{-11}$ cm^3/(molecule s), which is slightly less than the rate constant (k_2) for the simillar reaction C_2H_5 + Cl. Its value is consistent with the proposed mechanism of atom + radical disproportionation.

Acknowledgment. Acknowlegement is made to the Donors of the Petroleum Research Fund administered by the American Chemical Society, for the support of this research.

References and Notes

(1) Cohen, N.; Benson, S. W. *Chem. Rev.* **1993**, *93*, 2419. Cohen, N.; Benson, S. W. Thermochemistry of Alkanes and Cycloalkanes. Chapter 6 In *The Chemistry of Alkanes and Cycloalkanes*; Patai, S., Rappoport, Z., Eds.; John Wiley and Sons: New York, 1992.

(2) Golden, D. M.; Benson, S. W. *Chem. Rew.* **1969,** *69*, 125.

(3) Fettis, G. C.; Knox, J. H. The Rate Constant of Halogen Atom Reactions. In *Progress in Reaction Kinetics*; Porter, G., Ed.; 1964; Vol. 2, Chapter 1, p 3.

(4) Tsang, W. *Int. J. Chem. Kinet.* **1978**, *10*, 821.

(5) Tsang, W. *J. Am. Chem. Soc.* **1985**, *107*, 2872.

(6) Comprehensive evaluations can be found in, for example: O'Neal, H. E.; Benson, S. W. Thermochemistry of Free Radicals, Vol. 2, Chapter 17. In *Free Radical*; Kochi, J. K., Ed.; John Wiley and Sons: New York, 1973. Mc Millen, D. F.; Golden, D. M. *Annu. Rev. Phys. Chem.* **1982**, *33*, 493. Reference 2.

(7) Seakins, P. W.; Pilling, M. J.; Niiranen, J. T.; Gutman, D.; Krasnoperov, L. N. *J. Phys. Chem.* **1992**, *96*, 9847.

(8) Seetula, J. A.; Gutman, D. *J. Phys. Chem.* **1990**, *94*, 7529.

(9) Seetula, J. A.; Russell, J. J.; Gutman, D. *J. Am. Chem. Soc.* **1990**, *112*, 1347.

(10) Gutman, D. *Acc. Chem. Res.* **1990**, *23*, 375.

(11) King, K. D.; Golden, D. M.; Benson, S. W. *Trans Faraday Soc.* **1970**, *66*, 2794.

(12) Comber, J. W.; Whittle, E. *Trans. Faraday Soc.* **1966**, *62*, 2643.

(13) Fettis, G. C.; Trotman-Dickenson, A. F. *J. Chem. Soc.* **1961**, 3037.

(14) Fettis, G. C.; Knox, J. H.; Trotman-Dickenson, A. F. *J. Chem. Soc.* **1960**, 4177.

(15) Russell, J. J.; Seetula, J. A.; Gutman, D. *J. Am. Chem. Soc*. **1988**, *110*, 3092.
(16) Berkowitz, J.; Ellison, G. B.; Gutman, D. *J. Phys. Chem*. **1994**, *98*, 2744.
(17) Miyokawa, K.; Tschuikow-Roux, E. *J. Phys. Chem*. **1990**, *94*, 715.
(18) Chen, Y.; Rauk, A.; Tschuikow-Roux, E. *J. Phys. Chem*. **1991**, *95*, 9900. Chen, Y.; Tschuikow-Roux, E.; Rauk, A. *J. Phys Chem*. **1991**, *95*, 9832.
(19) McEwen, A. B.; Golden, D. M. *J. Mol. Struct*. **1990**, *24*, 357.
(20) Timonen, R. S.; Gutman, D. *J. Phys. Chem*. **1986**, *90*, 2987.
(21) Timonen, R. S.; Seetula, J. A.; Gutman, D. *J. Phys. Chem*. **1990**, *94*, 3005.
(22) Dobis, O.; Benson, S. W. *J. Am. Chem. Soc*. **1995**, *117*, 8171.
(23) Nicovich, J. M.; van Dijk, C. A.; Kreutter, K. D.; Wine, P. J. *J. Phys. Chem*. **1991**, *95*, 9890.
(24) Dobis, O.; Benson, S. W. *Int. J. Chem. Kinet*. **1987**, *19*, 691.
(25) Dobis, O.; Benson, S. W. *J. Am. Chem. Soc.* **1993**, *115*, 8798.
(26) Dobis, O.; Benson, S. W.; Mitchell, T. J. *J. Phys. Chem*. **1994**, *98*, 12284.
(27) Dobis, O.; Benson, S. W. *J. Am. Chem. Soc.* **1990**, *112*, 1023.
(28) In ref 22 the indices of α have a typographical error. The correct indexation is the present one.
(29) Dobis, O.; Benson, S. W. *J. Phys. Chem*. **1995**, *99*, 4986.
(30) Dobis, O.; Benson, S. W. *J. Phys. Chem. A*. **1997**, *101*, 1305.
(31) Nicovich, J. M.; Wine, P. H. *Int. J. Chem. Kinet*. **1990**, *22*, 379.
(32) Muller-Markgraf, W.; Rossi, M. J. *J. Phys. Chem*. **1991**, *95*, 825.
(33) Muller-Markgraf, W.; Rossi, M. J. *Int. J. Chem. Kinet*. **1995**, *27*, 403.
(34) Amphlett, J. C.; Whittle, E. *Trans. Faraday Soc*. **1968**, *64*, 2130.
(35) Rossi, M. J.; Golden, D. M. *Int. J. Chem. Kinet*. **1983**, *15*, 1283. Rossi, M. J.; Golden, D. M. *Int. J. Chem. Kinet*. **1979**, *11*, 969.
(36) Andersen, H. C.; Van Artsdalen, E. R. *J. Chem. Phys*. **1944**, *12*, 479.
(37) Benson, S. W. *Thermochemical Kinetics*, 2nd ed.; John Wiley: New York, 1976.
(38) Pacey, P. D.; Wimalasena, J. H. *J. Phys. Chem*. **1984**, *88*, 5657.
(39) Brouard, M.; Lightfoot, P. D.; Pilling, M. J. *J. Phys. Chem*. **1986**, *90*, 445.
(40) Hanning-Lee, M. A.; Green, N. J. B.; Pilling, M. J.; Robrtson, S. H. *J. Phys. Chem*. **1993**, *97*, 860. Lightfoot, P. D.; Pilling, M. J. *J. Chem. Phys*. **1987**, *91*, 3373.
(41) Baldwin, R. R.; Walker, R. W.; Walker, R. W. *J. Chem. Soc., Faraday Trans. 1* **1980**, *76*, 825.
(42) Seakins, P. W.; Pilling, M. J. *J. Phys. Chem*. **1991**, *95*, 9874.
(43) Benson, S. W. *Acc. Chem. Res*. **1986**, *19*, 335; *J. Phys. Chem*. **1985**, *89*, 4366.
(44) Armstrong, N.; Simmons, R. F. *Symp. (Int.) Combust. Proc*. **1973**, *14*, 143. Rebbert, R. E.; Lias, S. G.; Ausloos, P. *Int. J. Chem. Kinet*. **1973**, *5*, 893. Callear, A. B.; Smith, G. B. *Chem. Phys. Lett*. **1985**, *122*, 196.
(45) Russell, J. J.; Seetula, J. A.; Senkan, S. M.; Gutman, D. *Int. J. Chem. Kinet*. **1988**, *20*, 759.
(46) It is difficult to present kinetic data in graphic form that covers more than 2 decades in *k* without making experimental errors appear very small. Reduced Arrhenius plots overcome this problem. We believe that this is the first use of such plots.